

# Application of the *G-Scheme* to Reactive Systems

M. Valorani\* and S. Paolucci†

\* Sapienza, University of Rome, Rome, Italy

† University of Notre Dame Notre Dame, IN, USA

**Abstract**—The theory relevant to the *G-Scheme* framework is presented in a companion paper. Here, we will present results relevant to hydrocarbon kinetics, to a CSTR model involving CO/H<sub>2</sub> mixtures, and reactive systems described by PDEs to demonstrate the effectiveness of the method. We also present results obtained by combining a Wavelet Adaptive Multilevel Representation (WAMR) technique to define the spatial discretization of the model with the time integration carried out with the *G-Scheme*. This approach allows to obtain time accurate solutions of prescribed accuracy with a much lower number of space-time degrees of freedom.

## I. INTRODUCTION

The next frontier in numerical simulation involves multi-physics, multi-scale, multi-disciplinary problems. Disciplines eager of computing power range from genetics, earth climate, biology, energy and combustion, micro/nano science and technology, among the most prominent. This demand cannot be simply accommodated by progress achieved in computer power alone, but requires breakthroughs in physical-mathematical modeling and numerical/algorithmic developments. Indeed, solutions of reaction systems in general are computationally very expensive because of the presence of a very large range of scales. However, to within an arbitrary but fixed accuracy, there are in general very fast and very slow time scales whose contributions to the active dynamics is negligible. Recently, we presented a new methodology [1] that exploits this circumstance to design a numerical framework able to achieve adaptive reduction of the dynamical system based on accuracy requirements. As a result, the original problem not only becomes substantially smaller, but more importantly non-stiff. The frozen (slow) and near-equilibrium (fast) modes play crucial roles in defining the active (dynamic) subspace, and thus it is mandatory to account for their contributions. To demonstrate the effectiveness of the method, we will present results relevant to three different reactive systems, namely a Continuously Stirred Tank Reactor (CSTR) with a CO/H<sub>2</sub> mixture, the auto-ignition of hydrocarbon/air mixtures in homogeneous systems, and a reaction/diffusion system featuring limit cycle behavior. The reaction/diffusion system is solved by combining a Wavelet Adaptive Multilevel Representation (WAMR) technique [2][3][4] to define the spatial discretization of the model with the time integration carried out with the *G-Scheme*.

## II. BASIC CONCEPTS

The numerical technique proposed in [1], referred to as the *G-Scheme*, embodies both the model reduction and the subsequent numerical integration of the reduced set of Ordinary Differential Equations (ODEs). The *G-Scheme* exploits the circumstance that systems arising from large kinetic mechanisms contain a very large range of scales with the fastest scales having a dissipative nature. This property ensures that the actual dimension of the system becomes much smaller than the original size after a short initial transient period. This lower dimensional subspace, named Slow Invariant Manifold (SIM), is present if there exists a spectral gap of characteristic time scales that separates slow and fast components of the dissipative kinetic systems. In this case, the most relevant asymptotic behavior of the system is confined in the SIM or the limit attractor (for a system having nontrivial asymptotic kinetics), which is invariant and exponentially attracting. Consequently, model reduction can be achieved by filtering out the dynamically irrelevant degrees of freedom (irrelevancy is based on an accuracy requirement) associated with the fastest components characterized by the most negative characteristic time scales.

Ideally, one would like to decompose the tangent space  $\mathcal{T}_x$  at any point  $\mathbf{x} \in C \subset \mathbb{R}^N$  in  $N$  invariant subspaces, so that the dynamics within each invariant subspace is fully decoupled from all other invariant subspaces, and is associated with a single characteristic time scale. This goal is not easy to achieve. However, decomposing the tangent space in subspaces, not necessarily invariant, characterized by time scales of comparable magnitude is at the core of the *G-Scheme*. We assume that the tangent space  $\mathcal{T}_x$  can be decomposed as the sum of four subspaces,

$$\mathcal{T}_x = \mathbb{E} \oplus \mathbb{H} \oplus \mathbb{A} \oplus \mathbb{T},$$

where the active subspace  $\mathbb{A}$  contains all the current intermediate dynamic time scales, all scales faster and slower than the active ones are confined in the fast and slow subspaces  $\mathbb{T}$  and  $\mathbb{H}$ , respectively, and,  $\mathbb{E}$  is the linear subspace spanned by directions associated with invariants, if any exist.

At each point  $\mathbf{x}$  of the Chemical Composition Space (CCS), the *G-Scheme* introduces a curvilinear frame of reference, defined by a set of ortho-normal basis vectors, with corresponding curvilinear coordinates, which is tied to the decomposition of the tangent space in the four

subspaces. The evolution of the curvilinear coordinates associated with the subspace  $\mathbb{A}$  is described by  $N_A = \dim(\mathbb{A}) \leq N$  ODEs, whereas the variation of the curvilinear coordinates associated with the subspaces  $\mathbb{T}$  and  $\mathbb{H}$  are accounted for by applying  $N_T = \dim(\mathbb{T}) \geq 0$  and  $N_H = \dim(\mathbb{H}) \geq 0$  algebraic corrections derived from asymptotics of the original ODEs. Note that if we have  $N_E = \dim(\mathbb{E}) \geq 0$  invariants, they can be formally eliminated so that the dynamics is restricted to move in the subspace  $\mathbb{H} \oplus \mathbb{A} \oplus \mathbb{T}$  that satisfies the invariants exactly. Adjusting the active ODEs dynamically during time integration is the most significant feature of the *G-Scheme*, because the numerical integration of the state vector  $\mathbf{x} \in \mathbb{R}^N$  is obtained by solving a number of ODEs typically much smaller than  $N$ . The active ODEs evolve in  $\mathbb{A}$ , which is freed from fast scales, and thus they are non-stiff. They can be solved by resorting to any explicit time integration scheme (e.g., ERK). When compared to a standard BDF implicit scheme for stiff problems, the *G-Scheme* offers the advantage of requiring the solution of  $N_A$  explicit instead of  $N$  implicit ODEs, at the expense of identifying the time scales and computing the set of orthonormal basis vectors that define the curvilinear frame of reference.

#### A. Basis Vectors and Time Scales

Clearly, the success of the *G-Scheme* relies on the ability to identify a decomposition of  $\mathcal{T}_x$  which ensures minimal (ideally no) coupling among slow, fast, and active time scales. The problem of finding a frame of reference yielding the maximal degree of fast/slow decoupling can be approached by resorting to the CSP refinements procedure [5]. In this work, we identify the set of basis vectors  $\mathbf{a}_i$ , defining the mapping of the change of frame of reference, with the right eigenvectors of the Jacobian matrix  $J$  of the vector field related to the kinetic problem of interest, with the dual vectors  $\mathbf{a}^j$  coinciding with the left eigenvectors of  $J$ . This yields a leading order approximation of the CSP vectors [6]. As estimate of the characteristic time scales, we consider the magnitude of the reciprocal of the eigenvalues,  $\lambda_i$  of  $J$ . The ordering of the basis vectors is critical for proper decomposition. Here, we order the modes according to the magnitude of the complex eigenvalues, that is

$$0 = |\lambda_1| = \dots = |\lambda_E| < |\lambda_{E+1}| \leq \dots \leq |\lambda_{H-1}| \ll \\ \ll |\lambda_H| \leq \dots \leq |\lambda_T| \ll |\lambda_{T+1}| \leq \dots \leq |\lambda_N|,$$

where

$$\begin{aligned} 0 = |\lambda_1| = \dots = |\lambda_E| & \text{ identify the time scales in } \mathbb{E}, \\ |\lambda_{E+1}| \leq \dots \leq |\lambda_{H-1}| & \text{ identify the time scales in } \mathbb{H}, \\ |\lambda_H| \leq \dots \leq |\lambda_T| & \text{ identify the time scales in } \mathbb{A}, \\ |\lambda_{T+1}| \leq \dots \leq |\lambda_N| & \text{ identify the time scales in } \mathbb{T}. \end{aligned}$$

with  $N_E = E$ ,  $N_H = H - E - 1$ ,  $N_A = T - H + 1$ , and  $N_T = N - T$ . Note that, because of this ordering, (possibly complex) eigenvalues with both negative and positive real parts can be found in  $\mathbb{H}$  and  $\mathbb{A}$ , whereas we expect the eigenvalues in  $\mathbb{T}$  to have negative real

parts, since this is the distinguishing feature of the class of problems for which the *G-Scheme* is expected to perform efficiently. The ratios  $\epsilon_T \equiv |\lambda_T/\lambda_{T+1}| < 1$  and  $\epsilon_H \equiv |\lambda_{H-1}/\lambda_H| < 1$  are measures of the spectral gaps between active and fast subspaces, and slow and active subspaces, respectively. Since the *G-Scheme* approximates the contribution of the very slow and very fast time scales with asymptotic corrections, it is expected that its accuracy and efficiency will be higher for larger spectral gaps, that is for smaller values of  $\epsilon_T$  and/or  $\epsilon_H$ . The controlling (driving) time scale of the dynamics is given by the fastest of the (active) time scales present in  $\mathbb{A}$ , and will be of the order of  $\tau_T = 1/|\lambda_T|$ .

For the problems discussed below, the reference solutions are obtained with *DVODE* [7] set with a precision (or *rtol*) of  $10^{-8}$ , and accuracy (or *atol*) of  $10^{-14}$ . The calculations carried out with the *G-Scheme* use the explicit four-stage Runge-Kutta scheme (ERK4) to integrate the active dynamics, and, except where noted otherwise, *rtol* =  $10^{-4}$  and *atol* =  $10^{-14}$  are user-defined parameters defining the relative and absolute values, respectively, of the total variation of the state variable over the time interval. They are used to form a threshold vector  $\varepsilon^j(\Delta t)$  defined as

$$\varepsilon^j(\Delta t) \equiv \text{rtol}^j |x^j(t_{n+1})| + \text{atol}^j,$$

which is used to identify the integer indices  $H$  and  $T$  that enter in the definition of the dimensions of the subspaces  $\mathbb{A}$ ,  $\mathbb{H}$ , and  $\mathbb{T}$ .

### III. CSTR MODEL

As a test model featuring complicated nonlinear behavior we consider the isobaric CSTR system at very low pressure involving CO/H<sub>2</sub> kinetics proposed by Brad *et al.* [8]. The kinetic mechanism involves 11 species and 33 reactions. The set of ODEs involves 11 rate equations and the energy conservation equation for the molar concentrations and temperature representing the state of the CSTR. The equations, the constants, as well as all other constitutive relations are the same as in [8]. The CSTR is an open system which possesses three invariants, one for each atomic species, with characteristic time scales equal to the residence time  $t_R = 1$ .

The dynamics of this system features different types of asymptotic behavior (fixed point, limit cycle, and chaotic attractor). Here we report results of the *G-Scheme* under the conditions involving limit cycle behavior, corresponding to the initial condition  $\{p^0, T^0\} = \{14 \text{ torr}, 680 \text{ K}\}$ . The temperature evolutions along the periodic orbit is shown in Fig. 1. Although we do not present additional details on the solution, over each cycle one can note a very fast ignition phase, where both  $T$  and HO<sub>2</sub> peak, followed by a relaxation phase, during which HO<sub>2</sub> is consumed, and lastly a new re-generation phase, during which HO<sub>2</sub> is produced, with the latter two phases occurring at nearly isothermal conditions. The relative error in  $T$  is below 1% (not shown), the maximum value being attained during the explosive stage, whereas the

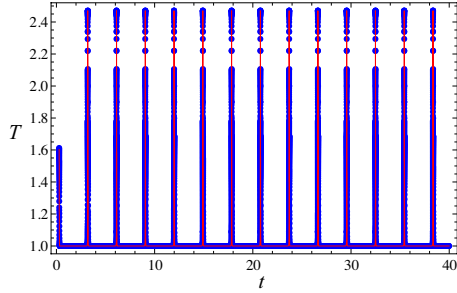


Fig. 1. Evolutions of  $T$  from *NDSolve* (line) and *G-Scheme* (points).

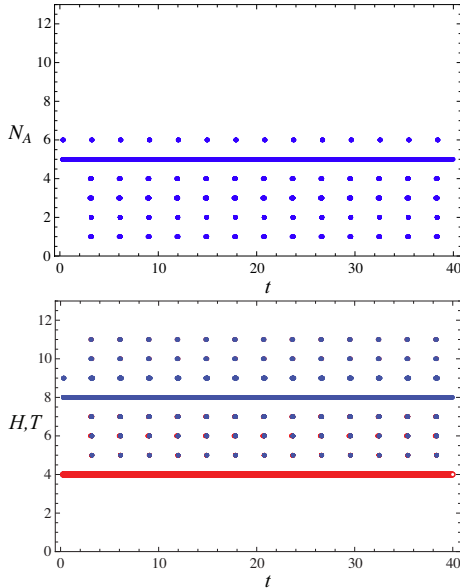


Fig. 2. Evolutions of number of active modes  $N_A$  (top), and  $H$  (red points) and  $T$  (blue points) indices (bottom).

error drops by several orders of magnitude during the relaxation and re-generation phases. The periodicity of the solution in Figs. 1 and of the number of active modes,  $N_A$ , shown in Fig. 2 demonstrates that the *G-Scheme* is able to provide repeatable sequences of the tangent space decomposition. The embedding dimension of the asymptotic dynamics of the CSTR model along the limit cycle, estimated as the  $\max(N_A)$  over a period is 6, whereas the average number of active equations weighed with respect to time, is approximately 5. Figure 3 (top) shows the time evolution of the integration time step, from which it is apparent that small time steps ( $\approx 10^{-5}$ ) are required for accuracy reasons in the ignition regime, and that large time steps ( $\approx 10^{-1.5}$ ) can be taken during the relaxation and re-generation phases. Figures 2 (bottom) and 3 (bottom) show that during the explosive regime both the  $T$  and  $H$  indices increase in such a way that their difference decreases. Thus, although the driving time scale  $\tau_T$  becomes small during the explosion stages because of the larger value of  $T$ , the degree of reduction increases, ( $N_A$  attains the value of unity). Instead, in-between two successive explosions,  $H$  and  $T$  attain constant values (4 and 8, respectively), so that  $N_A$  remains uniformly equal to 5. The analysis of the evolution of the time

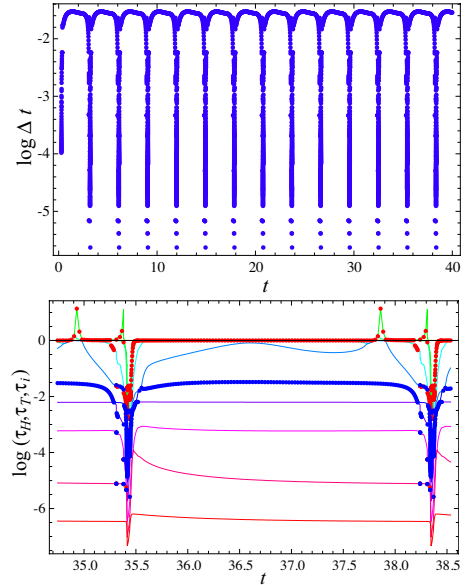


Fig. 3. Evolutions of integration time step (top), and the  $\tau_H$  time-scale (red points), the  $\tau_T$  time-scale (blue points), and all other time-scales (lines) (bottom).

rate of change of  $J$  demonstrates that the system has a nearly linear behavior (also confirmed in Fig. 3 (bottom) by the small changes in the time scales), whereas the nonlinearities are confined within the explosions.

#### IV. HYDROCARBON KINETICS

The *G-Scheme*'s performance is compared to that of the *DVODE* package, with reference to the auto-ignition process of stoichiometric mixtures of Methane/Air, Propane/Air, and n-Heptane/Air. The kinetic mechanisms considered are those of GRI 3.0 [9] (53 species; 325 reactions), Petersen *et al.* [10] (119 species; 665 reactions), and Curran *et al.* [11] (560 species; 2538 reactions), respectively. The initial temperature  $T_0$  is 750 K and  $p_0 = 1$  atm for all cases; they are chosen so as to yield a long ignition time which makes the auto-ignition very stiff<sup>1</sup>. The ratio of the reaction time  $\tau_{rea}$  to the ignition time  $\tau_{ign}$  for the tests considered is reported in Table I. Indeed, the *G-Scheme* is designed so as to be cost effective when the problem is stiff. The typical accuracy level produced by the *G-Scheme* can be appreciated by examining Fig. 4. The figure displays a trajectory of the constant volume, adiabatic, auto-ignition of a stoichiometric Propane/Air mixture, in a two-dimensional cross-section of the 119-dimensional CCS, and an enlargement of the temperature evolution near the ignition time. The figure indicates that the state values (points) found by the *G-Scheme* follow the reference trajectory quite accurately, and that a small time shift error ( $\approx 0.01$ ) develops in the prediction of the ignition time. The ratio of the average number of degrees of freedom,  $\langle N_A \rangle$  (average number of active ODEs per iteration step), integrated by the *G-Scheme* to

<sup>1</sup>Here we assume a measure of stiffness to be given by the ratio between the driving time scale during the ignition and the ignition time itself.

TABLE I

 $T_0 = 750 \text{ K}, p_0 = 1 \text{ ATM}, \text{ ALL CASES.}$ 

Mech	$\tau_{ign} [\text{s}]$	$\tau_{rea} [\text{s}]$	$\tau_{rea}/\tau_{ign}$	$N$	$\langle N_A \rangle$	$\langle N_A \rangle/N$
Methane	366.5	0.2	$5.46 \times 10^{-4}$	53	3.78	0.07
Propane	16.38	0.05	$3.05 \times 10^{-3}$	119	3.83	0.03
n-Heptane	$2.93 \times 10^{-1}$	$3.50 \times 10^{-3}$	$1.19 \times 10^{-2}$	560	41.11	0.07

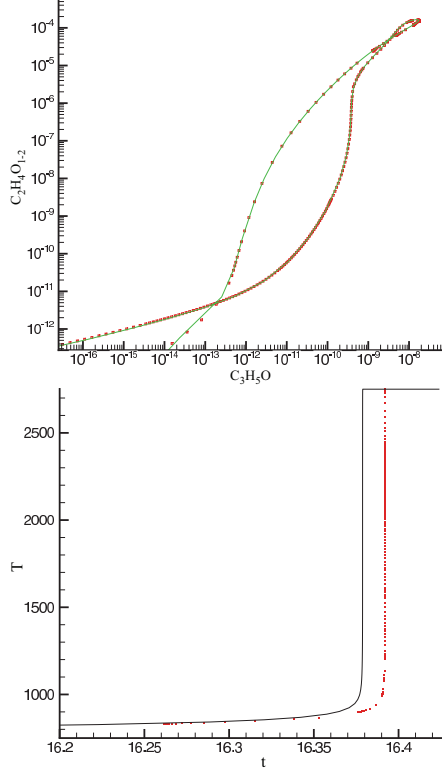


Fig. 4. Trajectory in CCS (left) and  $T$  evolution obtained for Propane/Air (right) with *DVODE* (solid line) and *G-Scheme* (red symbols).

the problem dimension,  $N$  (number of ODEs per iteration step), given in Table I, is a measure of the degree of (adaptive) reduction realized by the *G-Scheme*. Note that the degree of reduction is highly problem-dependent: for the cases studied, it is always below 10%. Figure 5 shows the time evolution of the active ( $N_A$ ), slow ( $N_H$ ), and fast ( $N_T$ ) subspace dimensions. Note that  $N_A$  is initially equal to  $N = 119$  (no reduction) and quickly drops below 5; later, it stays between 20 and 30 during the long nearly isothermal induction stage. It is noteworthy to observe that even during the explosion stage, when the temperature experiences the largest growth,  $N_A$  remains small because in this period most of the modes slower than the driving ones are essentially frozen, so  $H$  stays very close to  $T$ , and thus a small number of active modes are obtained. Finally,  $N_A$  attains a unit value while the kinetics approaches the equilibrium state at the slowest pace ( $\tau_T = \tau_{E+1}$ ). Figure 6 shows the time evolution of the time scales corresponding to modes  $H - 1$ ,  $H$ ,  $T$ ,  $T + 1$ , and  $N$ . The regions between  $\tau_{H-1}$  and  $\tau_H$ , and  $\tau_T$  and  $\tau_{T+1}$  represent the slow/fast gaps, respectively. During the induction stage and the equilibrium stage,

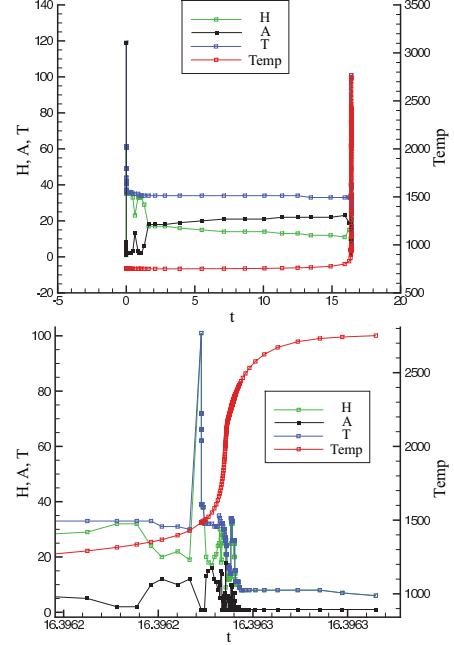


Fig. 5. Active  $N_A$  (black), slow  $N_H$  (green), and fast  $N_T$  (blue) subspace dimensions; induction stage (left); explosion stage (right).

the fast gap  $\epsilon_T$  is well developed and clearly identifiable, whereas the slow gap  $\epsilon_H$  is always rather narrow and mostly identified by the enforced error control. Note that during the explosion stage, the driving time scale attains its lowest value although the value of  $T$  keeps decreasing. This happens because the large growth in temperature induces a corresponding growth of the eigenvalues at all scales. Thus all active scales become smaller, albeit still confined in the range  $H - T \approx 10-40$ . The region between  $\tau_{T+1}$  and  $\tau_N$  represents the fast subspace. The ratio  $\tau_H/\tau_T$  is a measure of the stiffness of the reduced problem, which can be compared with the stiffness ratio of the original problem  $\tau_{E+1}/\tau_N$ , from which one can conclude that the reduced problem is significantly less stiff than the original. Finally, the time evolution of the integration time steps found by the *G-Scheme* and *DVODE* are shown in Fig. 7. Note that both histories follow a similar pattern with smaller steps during the initial transient and the explosion stage, and larger steps during the induction period and the approach to equilibrium.

## V. REACTION-DIFFUSION MODEL

As a typical reaction-diffusion model exhibiting a rich dynamic structure, we consider the model proposed by Elezgaray and Arneodo [12] (EA model). The EA model

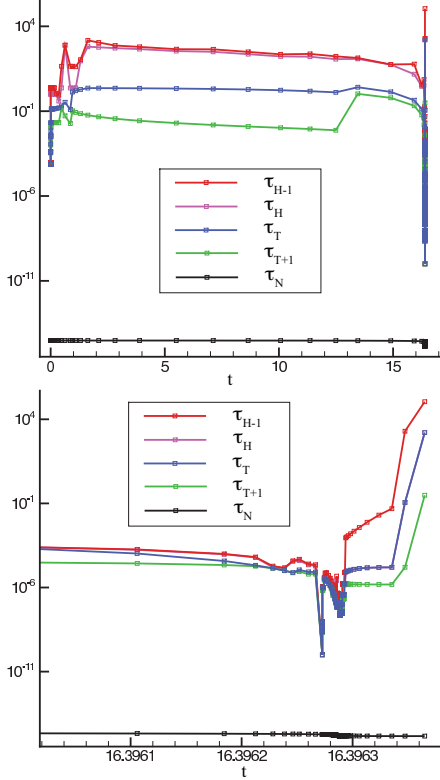


Fig. 6. Time scales and gaps: induction stage (top), explosion stage (bottom);  $\tau_H$  (slowest active scale);  $\tau_T$  (fastest active or driving scale); fastest scale  $\tau_N$  (black). Note that  $\epsilon_H = \tau_{H-1}/\tau_H$  and  $\epsilon_T = \tau_T/\tau_{T+1}$  measure the slow/fast gaps, respectively.

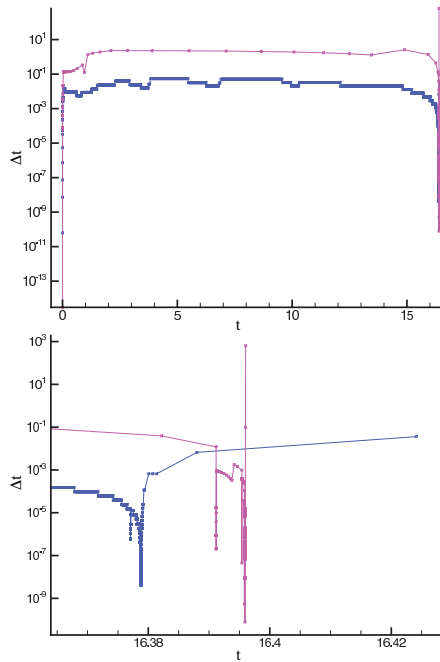


Fig. 7. Integration time step evolutions obtained with DVODE (blue) and *G-Scheme* (purple).

is a system of two coupled nonlinear PDEs:

$$\begin{aligned}\frac{\partial u}{\partial t} &= D \frac{\partial^2 u}{\partial x^2} + \epsilon^{-1} (v - (u^2 + u^3)), \\ \frac{\partial v}{\partial t} &= D \frac{\partial^2 v}{\partial x^2} - u + \alpha,\end{aligned}$$

in  $(u(x, t), v(x, t))$ ,  $(x, t) \in ([0, 1], [0, \infty))$ , representing the concentrations of two chemical species with an isothermal explosive kinetics displaying intermittent bursting for some values of the parameters. Here  $D$ ,  $\alpha$ , and  $\epsilon$  are positive parameters. The system is solved with initial conditions  $u(x, 0) = v(x, 0) = 0$  for  $x \in [0, 1]$ , and boundary conditions  $u(0, t) = u(1, t) = -2$  and  $v(0, t) = v(1, t) = -4$  for  $t > 0$ . For small and large values of diffusion  $D$ , the system stabilizes onto ignited and extinguished steady states, respectively. Intermediate values of  $D$  correspond to operating conditions that allow competition between the tendency to ignition due to the nonlinear kinetics, and the extinguishing behavior at the boundaries. This induces complex oscillations and intermittent bursting in the center of the spatial domain. In this case, no invariants are present, hence  $E = 0$ . The calculations refer to  $D = 0.032$ ,  $\alpha = 0.01$ , and  $\epsilon = 0.01$  so as to obtain a limit cycle behavior.

A Wavelet Adaptive Multilevel Representation (WAMR) technique [2][3][4] is used to provide the spatial discretization of the model. We analyzed this same model problem in [1], where a uniform mesh discretization was used. The time integration is obtained by both the *G-Scheme* and DVODE, and the two solutions are compared. To demonstrate the accuracy of the *G-Scheme*, we plot in Fig. 8 the evolutions of  $u$  at the mid-point  $x = 0.5$  and the corresponding phase trajectory's approach to the limit cycle as computed by DVODE and the *G-Scheme* with two different relative tolerances ( $rtol = 10^{-3}$  and  $10^{-4}$ ). The convergence of the *G-Scheme* solutions to the reference orbit is apparent, whereas a small time shift develops after 20 time units. In Fig. 9, we report the time evolution of the number of wavelet collocation points,  $N$ , and of the active modes  $N_A$  found by the *G-Scheme* when using the two tolerances. The number of collocation points at one time instant defines the minimum number of spatial degrees of freedom required to achieve the prescribed spatial accuracy. Similarly the number of active modes  $N_A$  defines the minimum number of temporal degrees of freedom required to achieve the prescribed temporal accuracy. The number of collocation points  $N$  during one cycle undergoes a slow growth up to about 260, followed by a rapid decrease down to about 120. In contrast, the number of active modes  $N_A$  remains rather constant during the slow growth of  $N$ , and develops two peaks a little earlier than the drop in  $N$ . The largest  $N_A$  is approximately 150, and the smallest is 10. The integration time step,  $\Delta t$ , used by the *G-Scheme*, oscillates between  $10^{-4}$  and  $10^{-1}$  as can be seen from Fig. 9.

In the present calculations, the coarsest spatial scale consists of 16 uniformly spaced collocation points, and

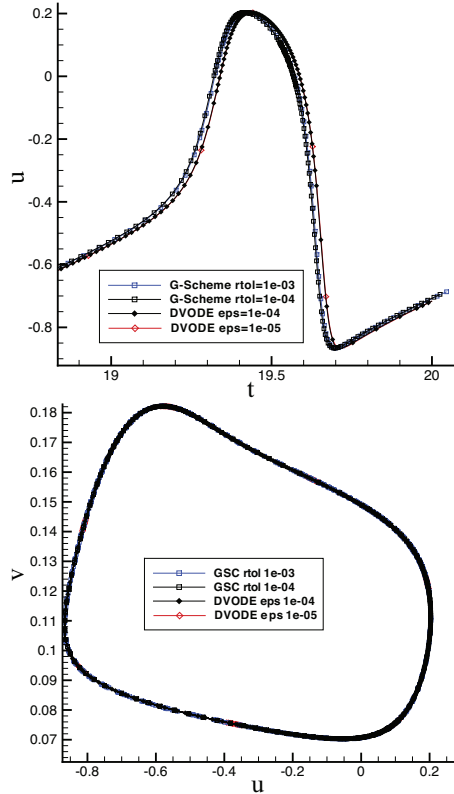


Fig. 8. Time evolution of  $u$  at  $x = 0.5$  (left), and trajectories in the  $(u-v)$ -plane, as computed by DVODE and  $G$ -Scheme with two different relative tolerances ( $rtol = 10^{-3}$  and  $10^{-4}$ ).

the spatial resolution is adaptively increased up to a resolution equivalent to a uniform mesh of  $16 \times 2^{10} = 16,384$  collocation points. With  $rtol = 10^{-4}$ , the number of integration steps required to reach 20 time units is 3,390, which is equivalent to a total number of space-time degrees of freedom (dof) of 111,083,520. It should be noted that in this problem we have two unknowns,  $u$  and  $v$ , for each spatial point. Instead, the dof required by the adaptive spatial discretization is 914,492, which implies a saving factor of 121.5. The actual number of equations solved by the  $G$ -Scheme with is 262,977, which involves a reduction by a factor of 3.5 with respect to using DVODE and of 422.4 with respect to using a uniform mesh of equivalent spatial accuracy. With  $rtol = 10^{-3}$ , the equivalent reduction factor is approximately 540. Thus, combining the adaptive wavelet technique with the  $G$ -Scheme allows to obtain a time accurate solution of prescribed accuracy with a much smaller number of space-time degrees of freedom.

## VI. ACKNOWLEDGEMENTS

MV acknowledges the support of the Italian Ministry of University and Research (MIUR) and the US Department of Energy, Office of Basic Energy Sciences, SciDAC Computational Chemistry Program. SP acknowledges the support of the University of Notre Dame and NSF (CBET-0650843) while working on the  $G$ -Scheme during his

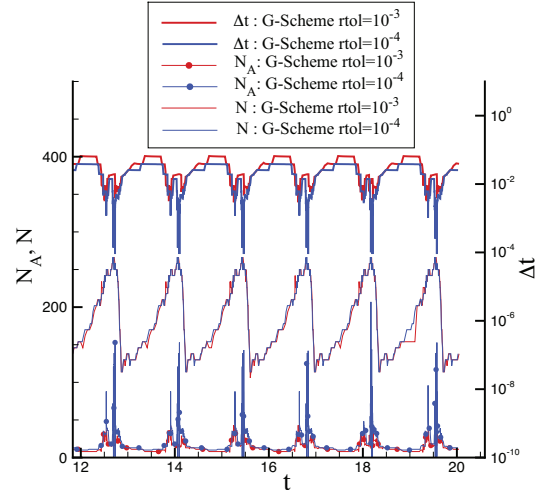


Fig. 9. Time evolution of the number of wavelet collocation points,  $N$ , and of the active modes,  $N_A$ , for two different relative tolerances ( $rtol = 10^{-3}$  and  $10^{-4}$ );  $\Delta t$  is the integration time step used by the  $G$ -Scheme.

stay at the University of Rome. We acknowledge the technical support of T. Grenga in the development of the FORTRAN porting of the  $G$ -Scheme, and of Z. Zicoski for the WAMR/ $G$ -Scheme merging and calculations.

## REFERENCES

- [1] M.Valorani, S.Paolucci, The  $G$ -Scheme: A framework for multi-scale adaptive model reduction, In print, J.Comp.Phys. (2009).
- [2] S.Singh, Y.Rastigejev, S.Paolucci, J.M.Powers, Viscous detonation in  $H_2-O_2-Ar$  using intrinsic low-dimensional manifolds and wavelet adaptive multilevel representation, Combust. Theory Modelling 5 (2001) 163–184.
- [3] Y.A.Rastigejev, S.Paolucci, Wavelet adaptive multiresolution representation: Applications to viscous multiscale flow simulations, Int. J. Wavelets Multiresolution and Information Processing 4 (2) (2006) 333–343.
- [4] Y.A.Rastigejev, S.Paolucci, Wavelet-based adaptive multiresolution computation of viscous reactive flows, Int. J. Num. Methods in Fluids 52 (7) (2006) 749–784.
- [5] S.H.Lam, D.A.Goussis, The CSP method for simplifying kinetics, International Journal of Chemical Kinetics 26 (1994) 461–486.
- [6] M.Valorani, D.A.Goussis, F.Creta, H.N.Najm, Higher order corrections in the approximation of low dimensional manifolds and the construction of simplified problems with the CSP method, J. Comput. Phys. 209 (2005) 754–786.
- [7] P.N.Brown, G.D.Byrne, A.C.Hindmarsh, VODE, A variable-coefficient ODE solver, SIAM Journal on Scientific and Statistical Computing 10 (5) (1989) 1038–1051.
- [8] R.B.Brad, A.S.Tomlin, M.Fairweather, J.F.Griffiths, The application of chemical reduction methods to a combustion system exhibiting complex dynamics, Proceedings of the Combustion Institute 31 (2007) 455–463.
- [9] G.P.Smith, D.M.Golden, M.Frenklach, N.W.Moriarty, B.Eiteneer, M.Goldenberg, C.T.Bowman, R.K.Hanson, S.Song, W. J. V.V.Lissianski, Q.Zhiwei, GRI mechanism for Methane/Air, Version 3.0. URL [www.me.berkeley.edu/gri\\_mech/](http://www.me.berkeley.edu/gri_mech/).
- [10] E.L.Petersen, D.M.Kalitan, S.Simmons, G.Bourque, H.J.Curran, J.M.Simmie, Methane/Propane oxidation at high pressures: Experimental and detailed chemical kinetic modeling, Proc. Combust. Inst 31 (2007) 447–454.
- [11] H.J.Curran, P.Gaffuri, W.J.Pitz, C.K.Westbrook,  $n$ -Heptane, detailed mechanism, Version 2 (2002). URL [www-cms.llnl.gov/combustion/combustion2.html](http://www-cms.llnl.gov/combustion/combustion2.html)
- [12] J.Elezgaray, A.Arneodo, Crisis-induced intermittent bursting in reaction-diffusion chemical systems, Phys. Rev. Lett. 68 (1992) 714–717.